FXYD5 promotes the growth of glioblastoma by targeting the PI3K/AKT/ACSL4 signaling axis

BANG WANG[1], YONG QIN[1], HANG CHENG[1], YIBIN ZENG[2], LIANGLEI JIANG[2] and XUEBIN HU[2]

[1]Department of Neurosurgery, Sinopharm Dongfeng General Hospital, Hubei University of Medicine, Shiyan, Hubei 442008, P.R. China; [2]Department of Neurosurgery, Union Hospital, Tongji Medical College, Huazhong University of Science and Technology, Wuhan, Hubei 430022, P.R. China

Received March 18, 2026; Accepted July 28, 2026

DOI: 10.3892/or.2026.9193

Abstract. Glioblastoma (GBM) is the most malignant primary brain tumor, with limited therapeutic options. Dysregulation of FXYD5 has been reported in multiple malignancies, suggesting FXYD5 as a potential target for precision medicine. In the present study, FXYD5 expression and prognostic significance were analyzed using biological analysis on multiple databases and it was identified that FXYD5 was observably upregulated in GBM and inversely correlated with the prognosis of patients. Functional studies were investigated in LN229 and U251 GBM cell lines through FXYD5 knockdown and overexpression approaches, assessing proliferation (Cell Counting Kit-8), apoptosis (flow cytometry), migration/invasion (Transwell assays) and lipid metabolism (free fatty acids, triglycerides, cholesterol, Nile Red staining). Knockdown of FXYD5 suppressed GBM cell proliferation, migration and invasion, while increasing apoptosis, indicating that FXYD5 may serve as a therapeutic target for GBM. Mechanistic studies examined the PI3K/AKT/long-chain acyl-coenzyme A (CoA) synthase 4 4 (ACSL4) pathway via western blotting and rescue experiments, finding that FXYD5 activated the PI3K/AKT signaling pathway, leading to upregulation of ACSL4 and enhanced lipid metabolism. *In vivo*, a subcutaneous xenograft mouse model was used to evaluate whether PI3K/AKT inhibition could antagonize FXYD5 overexpression-induced tumor growth and PI3K/AKT inhibition reversed FXYD5 overexpression-induced tumor growth in the subcutaneous mouse model. These findings revealed that FXYD5 promotes GBM progression via the PI3K/AKT/ACSL4 signaling axis and represents a potential therapeutic target for GBM.

Correspondence to: Dr Xuebin Hu, Department of Neurosurgery, Union Hospital, Tongji Medical College, Huazhong University of Science and Technology, 1277 Jiefang Avenue, Wuhan, Hubei 430022, P.R. China
E-mail: hxb7276@hust.edu.cn

Key words: FXYD5, PI3K/AKT, lipid metabolism, glioblastoma

Introduction

Glioblastoma (GBM) is an intrinsic brain tumor considered to originate from glial stem or progenitor cells; its incidence increases with age and is higher in males (1,2). Gliomas account for 30% of primary brain tumors and 80% of all malignant ones (3). GBM is the most prevalent and aggressive primary brain tumor in adults, characterized histopathologically by necrosis and endothelial proliferation, which confer the highest grade (grade IV) in the World Health Organization classification system (4). The median overall survival rate for GBM ranges from 14.6 to 20.5 months, with less than 5% of patients living 5 years after diagnosis (5,6). Standard treatments, including surgical resection and chemoradiation, have not substantially improved long-term survival rates, and immunotherapeutic strategies have emerged as promising alternatives (7,8). Therefore, an improved understanding of clinical treatment challenges and therapeutic target is essential for GBM precision therapy.

The FXYD domain-containing ion transport regulator 5 (FXYD5) gene acts as a pro-oncogenic factor, as its expression promotes metastasis in multiple tumors, including endometrial, ovarian, pancreatic and lung cancers (9-11). In comparison to normal tissues, FXYD5 expression was elevated in various cancerous tissues (12). Furthermore, FXYD5 overexpression was typically anticipative of poor patient survival (10). Previous studies found that the metastatic tumors had higher expression of FXYD5 than the original tumors, and blocking FXYD5 expression stopped cancer cells from invading, spreading and proliferating (13-15). Thus, the authors' hypothesis is that FXYD5 has a significant impact on both development and metastasis in GBM. These findings suggest that high FXYD5 expression contributes to GBM pathogenesis and that FXYD5-targeted therapy represents a promising therapeutic strategy.

Long-chain acyl-coenzyme A (CoA) synthase 4 (ACSL4), an enzyme that esterifies CoA into certain polyunsaturated fatty acids, such as arachidonic acid and adrenic acid, could contribute to the execution of ferroptosis by triggering phospholipid peroxidation (16). Furthermore, fatty acid metabolism is crucially regulated by ACSL4, which also controls steroidogenesis, balances eicosanoid production, and may alter the phospholipid makeup of cell membranes (16). A

previous study has confirmed that inhibiting ACSL4 is associated with a reduction in phospholipids within mitochondrial membranes, enhancing cancer cell apoptosis (17). Lipidomic study further revealed that activated ACSL4 catalyzes polyunsaturated fatty acid-containing lipid formation (18). Moreover, ACSL4 could trigger metastatic extravasation by enhancing membrane fluidity and cellular invasiveness, promoting tumor development (19).

In the present study, it was found that the FXYD5 was upregulated and was essential for the survival and invasion of GBM. Mechanically, it was identified that FXYD5 boosted the expression of ACSL4 and increased the level of survival-promoting lipid metabolism, which contributed to development and migration of GBM cells. It was also revealed that FXYD5 could increase the expression of ACSL4 by activating the PI3K/AKT pathway, leading to higher lipid metabolism levels in GBM cells. Briefly, a potential new strategy to improve GBM treatment effectiveness via the FXYD5/PI3K/AKT/ACSL4 signal pathway was provided.

Materials and methods

Cell culture. LN229 and U251 were purchased from the Chinese Academy of Sciences Cell Bank and cultured in DMEM (cat. no. C11995500BT; Gibco; Thermo Fisher Scientific, Inc.) with 10% FBS (cat. no. 10099-141; Gibco; Thermo Fisher Scientific, Inc.) and 1% penicillin-streptomycin (cat. no. 15-140-122; Gibco; Thermo Fisher Scientific, Inc.). These cells were cultured in a 37˚C cell incubator with 5% CO_2 and were typically passaged every 2 days, with the passage ratio ranging from 1:2 to 1:3. In addition, the mycoplasma test results of the 2 cell lines were negative, and STR analysis confirmed that LN229 and U251 were consistent with DNA profiles reported by ATCC and indicated no other human cell line contamination.

Gene knockdown and overexpression. For gene knockdown, the short hairpin RNA (shRNA) was based on the lentiviral vector pLKO.1-puro with a U6 promoter. Target sequences were as follows: shNC (5'-GCGTGATCTTCACCGACA AGA-3'), shFXYD5 #1 (5'-CGTTGAAAGATACCACGT CCA-3'), shFXYD5 #2 (5'-GAGACACACAAGAGCACC AAA-3') and shACSL4 (5'-CGCTGCGTGAACGAGGGC TAT-3').

For FXYD5 overexpression, the full length coding sequence of human FXYD5 isoform 1 (RefSeq accession no. NM_014164.6) was cloned into the PCDH-CMV-EF1A-T2A-PURO vector. A non-targeting shRNA and the corresponding empty pCDH vector were used as the knockdown and overexpression controls, respectively. Lentiviruses were generated in 293T cells using the cloned vectors and a second-generation lentiviral packaging system (target plasmid: psPAX2: pMD2.G: polyethylenimine=3: 2: 1:12). 293T cells were seeded at 4x10^6 cells per 10-cm culture dish and cultured at 37˚C in a humidified atmosphere containing 5% CO_2 until they reached approximately 70-80% confluence. For each dish, 3 μg transfer plasmid, 2 μg psPAX2 packaging plasmid and 1 μg pMD2.G envelope plasmid were mixed in DMEM. Linear polyethyleneimine (BIOHUB 78PEI MAX 40K, cat. no. 78pei40000) was added at 12 μg per dish, corresponding to a total DNA-to-PEI mass ratio of 1:2. The DNA-PEI complexes were incubated for 20 min at room temperature, added dropwise to the cells and incubated at 37˚C for 6 h, after which the transfection medium was replaced with fresh complete medium.

Viral supernatants were collected at 48 and 72 h after transfection. The supernatant collected at 48 h was maintained at 4˚C until it was pooled with the 72-h harvest. The pooled supernatants were passed through a 0.45-μm filter to remove cells and cellular debris and were used immediately for transduction. As unconcentrated viral supernatants were used directly, the functional viral titers were not independently determined, and an MOI was not calculated.

For lentiviral transduction, LN229 and U251 cells were seeded in 6-well plates at a density of $5x10^5$ cells/well 24 h before transduction. The culture medium was then replaced with 2 ml fresh complete medium containing 500 μl of the corresponding viral supernatant and 8 μg/ml polybrene (cat. no. TR-1003; MilliporeSigma). The same number of target cells and the same volume of viral supernatant were used for the corresponding experimental and control groups. The cells were incubated with the viral supernatant at 37˚C in a humidified atmosphere containing 5% CO_2 for 24 h, after which the virus-containing medium was replaced with fresh complete medium.

At 48 h after transduction, puromycin selection was initiated using 2 μg/ml puromycin for LN229 cells and 1.5 μg/ml puromycin for U251 cells. Selection was continued for 72 h, with the corresponding untransduced cells cultured in parallel to confirm the effectiveness of selection. The surviving cells were subsequently allowed to recover in complete medium for 72 h before functional experiments. FXYD5 knockdown or overexpression efficiency was confirmed by reverse transcription-quantitative PCR and western blotting before the cells were used in subsequent assays. Cells transduced with the non-targeting shRNA lentivirus or the corresponding empty-vector lentivirus were used as the knockdown and overexpression controls, respectively.

RNA extraction and reverse transcription-quantitative PCR (RT-qPCR). Total RNA was extracted using TRIzol (cat. no. 15596026CN; Thermo Fisher Scientific, Inc.). Reverse transcription of total RNA was performed using reverse transcription kits (cat. no. R233-01; Vazyme Biotech Co., Ltd.). The experimental procedures were carried out in accordance with the manufacturer's instructions. qPCR was conducted using Taq Pro Universal SYBR qPCR Master Mix (cat. no. Q712-02; Vazyme Biotech Co., Ltd.). The thermocycling conditions were as follows: Initial denaturation at 95˚C for 30 sec, followed by 40 cycles of denaturation at 95˚C for 5 sec and annealing/extension at 60˚C for 30 sec. The relative expression of mRNA was quantified using the $2^{-\Delta\Delta Cq}$ method (20). Total RNA was extracted from three independent cell culture preparations (biological replicates). For each biological replicate, qPCR was performed in triplicate technical repeats for each gene.

The primers were as follows: H-GAPDH forward, 5'-TCC ATGACA ACTTTGGTATC-3' and reverse, 5'-CAGGGA TGATGTTCTGGA-3'; FXYD5 forward, 5'-AAAGATACC ACGTCCAGTTC-3' and reverse, 5'-CTGGAGTTCTGTGTA

GACTG-3'; ACSL4 forward, 5'-ATTGGTGGACAGAAC ATCTC-3' and reverse 5'-CTCCTGCTTGTAACTTCACT-3'; H-glycerol-3-phosphate acyltransferase 3 (GPAT3) forward, 5'-ACTTTAGAGTGGGCCACAATACG-3' and reverse, 5'-TGGGTGACTCATCTCTTTGGAT-3; and H-sterol O-acyltransferase 1 (SOAT1) forward, 5'-CAAGGCGCTCTC TCTTAGATG-3' and reverse, 5'-GGTCCAAACAACGGT AGGAAA-3'.

Western blot analysis. Cell lysates were prepared at 4˚C using a RIPA lysis buffer supplemented with 1X phosphatase inhibitors and 1X protease inhibitors (cat. no. 89901; Thermo Fisher Scientific, Inc.) and were quantified by the BCA Protein Assay Kit (cat. no. MA0082; Dalian Meilun Biology Technology Co., Ltd.). Protein samples containing 20 μg total protein per lane were mixed with 5X SDS-PAGE sample loading buffer (cat. no. P0015L; Beyotime Institute of Biotechnology) at a sample-to-buffer volume ratio of 4:1, yielding a final loading-buffer concentration of 1X. The samples were denatured at 95˚C for 10 min, separated using 10% SDS-PAGE and transferred onto 0.22-μm PVDF membranes. Protein lysates were prepared from three independent cell culture preparations (biological replicates). For each biological replicate, Western blotting was performed once, and the blots were imaged.

Western blotting was performed following a standardized protocol. Membranes were later blocked in 5% non-fat milk at room temperature for 2 h and incubated at 4˚C overnight with primary antibodies. Primary antibodies included anti-FXYD5 antibody (cat. no. BD-PN2424; Biodragon), anti-ACSL4 antibody (cat. no. 22401-1-AP; Proteintech Group, Inc.), anti-GPAT3 antibody (cat. no. 20603-1-AP; Proteintech Group, Inc.), anti-SOAT antibody (cat. no. ab307597; Abcam), anti-PI3K antibody (cat. no. 4249), anti-phospho-PI3K antibody (cat. no. 13857, Cell Signaling Technology, Inc.), anti-AKT antibody (cat. no. 4691, Cell Signaling Technology, Inc.), anti-phospho-AKT antibody (cat. no. 4060; all from Cell Signaling Technology, Inc.) and anti-GAPDH antibody (cat. no. 60004-1-Ig; Proteintech Group, Inc). The aforementioned antibodies were used at 1:1,000 dilution. Anti-rabbit secondary antibody (cat. no. ab6721; Abcam) and anti-mouse secondary antibody (cat. no. ab205719; Abcam) were used at a dilution of 1:3,000. Blots were used with Super ECL Detection Reagent (cat. no. 36208ES76; Shanghai Yeasen Biotechnology Co., Ltd.) for detection and the ChemiDoc XRS+ System for densitometric analysis of the images. Western blot bands were quantified using ImageJ software (version 1.54g; National Institutes of Health). The intensity of each target protein band was normalized to the corresponding GAPDH band from the same sample. Relative protein expression was calculated as the ratio of normalized target protein intensity in the experimental group to that in the control group.

Cell Counting Kit 8 assay. LN229 and U251 cells in the logarithmic growth phase were seeded into 96-well flat-bottom plates at a density of $2x10^3$ cells per well in 100 μl of complete DMEM containing 10% FBS. The plates were incubated at 37˚C in a 5% CO_2 humidified atmosphere for the indicated time periods (1, 2, 3, 4, and 5 days). At each time point, 10 μl of CCK-8 solution (cat. no. MA0218; Dalian Meilun Biology Technology Co., Ltd.) was added to each well, and the plates were incubated at 37˚C for an additional 2 h in the dark. The OD value was detected using a microplate reader (Countess 3; Thermo Fisher Scientific, Inc.) at 450 nm. Each experimental group contained six replicate wells per time point, and each experiment was performed in three independent biological replicates. The relative cell proliferation fold change was calculated as the ratio of OD_{450} value at each time point to that measured at 24 h (Day 1) for the same group.

Apoptosis assay. Cell apoptosis was assessed using an Annexin V-FITC Apoptosis Detection Kit (cat. no. C1062M; Beyotime Institute of Biotechnology) according to the manufacturer's instructions. LN229 and U251 cells were harvested 72 h after transduction, washed once with phosphate-buffered saline (PBS; pH 7.4), and resuspended in the binding buffer supplied with the kit at a density of $1x10^6$ cells/ml. Subsequently, 100 μl of the cell suspension, containing ~$1x10^5$ cells, was transferred to a flow cytometry tube and sequentially stained with 5 μl Annexin V-FITC and 10 μl propidium iodide (PI). The samples were gently mixed and incubated at room temperature in the dark for 15 min. Following incubation, 400 μl binding buffer was added to each tube, and the samples were immediately analyzed using a BD Accuri C6 Plus flow cytometer (BD Biosciences). Annexin V-FITC and PI fluorescence signals were recorded using the FITC-A and PE-A parameters, respectively. At least 10,000 events were acquired for each sample. Annexin V-$FITC^-$/PI^- cells were classified as viable cells, Annexin V-$FITC^+$/PI^- cells as early apoptotic cells, Annexin V-$FITC^+$/PI^+ cells as late apoptotic cells, and Annexin V-$FITC^-$/PI^+ cells as necrotic cells. The total apoptotic rate was calculated as the sum of the percentages of early and late apoptotic cells. The experiment was performed using three independent biological replicates.

Migration and invasion assay. For the migration assay, uncoated Transwell inserts were used. For the invasion assay, Corning Matrigel Basement Membrane Matrix (cat. no. 356234; Corning, Inc.) was thawed overnight on ice at 4˚C. All pipette tips, tubes and serum-free DMEM that came into contact with Matrigel were pre-cooled, and Matrigel was maintained on ice throughout dilution and coating to prevent premature polymerization. Matrigel was diluted to 200 μg/ml using ice-cold serum-free DMEM, and 100 μl diluted Matrigel was carefully added to the upper surface of each Transwell membrane. The coated inserts were incubated at 37˚C in a humidified atmosphere containing 5% CO_2 for 2 h to allow polymerization. Any residual liquid was carefully aspirated without disturbing the Matrigel layer, and the membrane was not allowed to dry before cell seeding.

LN229 and U251 cells were resuspended in serum-free DMEM and seeded into the upper chambers at a density of $1x10^5$ cells in 100 μl medium per insert. A total of 600 μl DMEM medium with 30% FBS (serum concentration selection was only a preliminary optimization experiment; 30% FBS was selected after preliminary optimization comparing 10, 20, and 30% FBS in LN229 and U251 cells; and that 30% FBS produced baseline migration with an adequate dynamic range for detecting inhibitory effects) in the lower chamber (Source of the method: Cloud-Clone Corp, IS079 Cell Invasion Assay Service Protocol, 2016). After 24 h at 37˚C in a 5% CO_2 atmosphere, the medium

was removed from the upper chamber, and non-migratory cells were removed with cotton swabs. Then migratory cells were fixed by 4% Tissue Fix Solution (cat. no. MA0192; Dalian Meilun Biology Technology Co., Ltd.) at room temperature (25˚C) for 20 min, stained by 0.1% crystal violet ammonium oxalate solution (cat. no. G1063; Beijing Solarbio Science & Technology Co., Ltd.) at room temperature (25˚C) for 15 min in the dark. Following washing and air-drying, stained cells were imaged using a light microscope and quantified stained areas using ImageJ. Migration was quantified by counting the number of cells per field (3 random fields per membrane). Each experimental group has 3 technical replicates.

Lipid assay. Lipid abundance and evaluation were examined by the Lipid Droplets Red Fluorescence Assay Kit with Nile Red (cat. no. C2051S; Beyotime Institute of Biotechnology). Moreover, free fatty acids were detected by the Amplex Red Free Fatty Acid Assay Kit (cat. no. S0215S; Beyotime Institute of Biotechnology). The contents of total cholesterol (TC) and triglyceride (TG) in LN229 cells or U251 cells were analyzed using the corresponding commercial kit according to the manufacturer's protocols (cat. nos. MB-3634A and MB-3858A; MEIBIAO; http://www.mbbiology.com/index.asp). Each experimental group has three technical replicates.

Immunoprecipitation (IP) assay. To determine whether FXYD5 physically associates with the PI3K complex, IP assays were performed in FXYD5-overexpressing LN229 and U251 cells. Cells were lysed in IP lysis buffer supplemented with protease and phosphatase inhibitors (cat. no. 89901; Thermo Fisher Scientific, Inc.). Lysates were incubated on ice for 30 min with intermittent vortexing, centrifuged at 14,000 x g at 4˚C for 15 min, and the supernatant was collected. Protein concentration was determined using the BCA Protein Assay Kit (cat. no. MA0082; Dalian Meilun Biology Technology Co., Ltd.). For each IP reaction, 500 μg of total protein was pre-cleared with 20 μl of Protein A/G agarose beads (cat. no. 20421; Thermo Fisher Scientific, Inc.) at 4˚C for 1 h, then incubated with 2 μg of anti-FXYD5 antibody (cat. no. BD-PN2424; Biodragon) or 2 μg of rabbit IgG (cat. no. ab171870; Abcam) as a negative control at 4˚C overnight. Subsequently, 30 μl of Protein A/G agarose beads was added and incubated at 4˚C for 2 h. The beads were washed five times with IP lysis buffer, and bound proteins were eluted by boiling in 2X SDS loading buffer at 95˚C for 10 min. The immuno-precipitates were analyzed by western blotting with antibodies against FXYD5, PI3K-p85 (cat. no. 4257; Cell Signaling Technology, Inc.), and PI3K-p110α (cat. no. 4249; Cell Signaling Technology, Inc.). The input lysate (5% of the IP reaction, 25 μg) served as a positive control.

Bioinformatic analysis. A total of 3 publicly available GBM datasets were analyzed: The Cancer Genome Atlas (TCGA)-GBM dataset, the GSE4290 dataset (21) and the China Glioma Genome Atlas (CGGA)-mRNAseq_693 dataset (22), in which GSE4290 dataset and the CGGA-mRNAseq_693 dataset were used for validation.

The GSE4290 dataset has 23 samples from epilepsy patients used as normal samples, 26 astrocytoma, 50 oligodendrogliomas, and 81 GBMs. This dataset was annotated and 77 cases of grade 4 tumor samples were obtained using the GPL570 platform (https://www.ncbi.nlm.nih.gov/geo/query/acc.cgi?acc=GPL570). In addition, the tumor samples were supplemented with 31 cases of grade 3 samples and 45 cases of grade 2 samples, totaling 153 tumor samples.

Furthermore, a total of 646 gene expression matrices for patients with glioma and clinical information from the CGGA-mRNAseq_693 dataset were obtained, including 398 primary patients and 248 recurrent patients, to analyze the expression levels of FXYD5 in primary and recurrent patients.

The TCGA-GBM dataset obtained 149 samples, of which 5 samples were normal brain tissue samples and 144 samples were tumor samples. Based on the gene expression level (TPM value) of FXYD5, the 144 patients in TCGA-GBM were classified using the strategy with the smallest P-value, obtaining the FXYD5 high-expression group (106 cases) and the FXYD5 low-expression group (38 cases). The cutoff value was 30.00632, which was determined using the surv_cutpoint function from the 'survminer' R package (https://github.com/kassambara/survminer), which maximizes the log-rank test statistic.

The following are the precise steps for using Gene Ontology (GO) enrichment analysis to uncover phenotypes (lipid metabolism) associated with FXYD5: The DESeq2 package (version 4.4.2) (23) in R was used for differential analysis based on the high-expression and low-expression patient groups of FXYD5 (TCGA-GBM dataset). The criterion was |log2FoldChange|>1 with an adjusted P<0.05. A total of 867 upregulated and 105 downregulated genes were identified.

Furthermore, the ssGSEA method was employed to validate the link between FXYD5 and lipid metabolism. The precise processes were as follows: Using the MSigDB database's c2.all.v7.4. symbols gene set and the R (version 4.4.2) package GSVA (24) to quantitatively assess the lipid metabolism levels of 144 patients in the TCGA-GBM dataset.

The gene with the strongest association to FXYD5 was found, and FXYD5-related differentially expressed genes were mapped onto lipid metabolism-related genes (statistical method: T-test). ACSL4, GPAT3 and SOAT1 were the most critical (decided by gene background function) and showed a connection with FXYD5 gene expression levels greater than 0.3 (statistical method: Pearson correlation coefficient), indicating a significant relationship.

Animal models. All animal procedures were approved by the Hubei Provincial Center for Disease Control and Prevention (approval no. 202510218; Wuhan, China). Male BALB/c nude mice, aged 4-5 weeks and weighing ~18 g at the start of the experiment, were procured from Gem Pharmatech LLC for the study *in vivo*. Mice were maintained under controlled environmental conditions with a temperature of 22±2˚C, relative humidity of 55±5%, and a 12/12-h light/dark cycle (lights on from 07:00 to 19:00). All mice were housed in individually ventilated cages (IVC) with sterile corncob bedding, at a maximum density of five mice per cage, and were provided with sterilized standard rodent chow and autoclaved drinking water ad libitum. Cage bedding, food, and water were changed twice weekly. A total of 20 mice were randomized into four groups (Vector group, OE-FXYD5 group, AKT inhibitor group and OE-FXYD5 group + AKT

inhibitor group) under a double-blind protocol. The Vector group received vector-control LN229 cells using empty PCDH-CMV-EF1A-T2A-PURO vector; the OE-FXYD5 group received FXYD5-overexpressing LN229 cells plus vehicle; the AKT inhibitor group received vector-control LN229 cells plus AKT inhibitor; and the OE-FXYD5 + AKT inhibitor group received FXYD5-overexpressing LN229 cells plus AKT inhibitor. LN229 cells from vector control, FXYD5-overexpressing (OE-FXYD5), and control groups were cultured in DMEM with 10% FBS until reaching 80-90% confluence. On the day of injection, cells were trypsinized (0.25% trypsin-EDTA), washed twice with sterile PBS (centrifugation at 300 g for 5 min), and resuspended in serum-free DMEM at a concentration of $3x10^7$ cells/ml. A volume of $3x10^6$ LN229 cells in PBS was subcutaneously injected using a 100-μl needle into the right flank of the mouse (n=5 per group). The AKT inhibitor, (E)-Akt inhibitor-IV (100 μmol/kg; cat. no. 959841-49-7; Targetmol), was dissolved in DMSO to prepare a stock solution of 50 mM, and the stock was then diluted in sterile PBS to achieve a final working concentration of 100 μmol/kg body weight, with a final DMSO concentration of 0.1% (v/v). For the control groups (Vector and OE-FXYD5 groups), mice received an equal volume of vehicle solution (0.1% DMSO in PBS) by the same route of administration on the same schedule. The AKT inhibitor group and OE-FXYD5 + AKT inhibitor group received the inhibitor solution as described. All injections were performed subcutaneously at the same site (the left flank) on days 21, 25, and 29 post-cell inoculation.

Tumor length (L) and width (W) were measured every 4 days starting from day 13 after cell inoculation using a digital caliper. Tumor volume was calculated using the formula: Volume=$LxW^2/2$. Measurements were performed by two independent investigators blinded to the group allocation. The average of the two measurements was recorded.

At the experimental endpoint (day 33 post-inoculation) or when tumors reached the humane endpoint of 2,000 mm^3, mice were euthanized by intraperitoneal injection of pentobarbital sodium at a lethal dose of 150 mg/kg body weight. Death was confirmed by permanent cessation of heartbeat and respiration, followed by cervical dislocation as a secondary physical method to ensure permanent death, in accordance with the AVMA Guidelines for the Euthanasia of Animals. All personnel performing euthanasia were trained and certified in rodent handling and euthanasia techniques.

The final tumor volume measured at day 33 (or at euthanasia if earlier) was used for analysis. For animals euthanized before day 33 due to tumor size limits, the last measured volume was carried forward for longitudinal analysis. The tumors were then extracted and fixed for immunohistochemistry.

Immunohistochemical (IHC) analysis. The tissues were dewaxed with dimethylbenzene and rehydrated with 100-95-85-70% alcohol. The tissues were blocked with 3% H_2O_2 before being treated with 5% citric acid buffer (pH=6.0) at 100˚C for 20 min to retrieve antigens. Then, bovine serum albumin (cat. no. A8020; Beijing Solarbio Science & Technology Co., Ltd.) was added to prevent nonspecific binding. Subsequently, the primary antibodies anti-FXYD5 (1:200; cat. no. 12166-1-AP; Proteintech Group, Inc.), anti-phospho-AKT (Ser473) (1:200; cat. no. 4060; Cell Signaling Technology, Inc.) and anti-ACSL4 (1:200; cat. no. 22401-1-AP; Proteintech Group, Inc.) were incubated at 4˚C overnight, then incubated at room temperature with the corresponding horseradish peroxidase-conjugated goat anti-rabbit IgG secondary antibody (1:500; cat. no. ab6721; Abcam) for 1 h and finally treated with 2,4-diaminobenzidine. Finally, the sections were re-stained with Mayer's hematoxylin. All stained sections were observed and imaged using a light microscope (Olympus BX53; Olympus Corporation) equipped with a digital camera (DP73; Olympus Corporation).

Negative controls (NC) were performed by substituting the primary antibody with isotype-matched non-immune rabbit or mouse IgG at the same concentration. All NC staining was processed in parallel with experimental samples.

Whole tumor sections were scanned using a digital slide scanner. A total of 3 random fields were selected from each tumor section, avoiding necrotic areas. For each field, the percentage of positively stained cells and staining intensity were assessed by two independent observers blinded to group allocation.

Statistical analysis. Each section describes the specific statistical analysis. For the cell experiments, the statistical differences between the two groups were determined using the unpaired Student's t-test. When more than two groups were involved, one-way analysis of variance was used followed by Tukey's multiple-comparisons test. Unless otherwise stated, three independent repeated experiments were conducted for each case, and the data were presented as the mean ± standard deviation. Statistical analysis was performed using GraphPad Prism 9 (Dotmatics). $P<0.05$ was considered to indicate a statistically significant difference.

Results

FXYD5 is upregulated and is a potential therapeutic target in GBM with dismal prognosis in patients. To identify potential targets for the treatment of GBM, gene expression profiles between normal tissue and GBM tumor tissue were analyzed. FXYD5 has been reported showing significantly increased expression in tumors (25). The GSE4290 dataset and CGGA-mRNAseq_693 dataset indicated a significant increase in FXYD5 mRNA levels in GBM tissue compared with normal tissue and in recurrent patients compared with primary patients (Fig. 1A). Besides, 23 samples from patients with epilepsy were obtained and used as non-tumor samples. A total of 157 tumor samples, including 26 astrocytomas, 50 oligodendrogliomas and 81 GBMs were obtained from the GSE4290 dataset and it was found that FXYD5 was highly expressed in astrocytoma and patients with GBM, and it reached the highest level in patients with GBM (Fig. S1A). As the glioma progressed, the expression level of FXYD5 also gradually increased (Fig. S1B). Importantly, patients with GBM with higher FXYD5 expression were more prone to adverse events and had shorter survival time than patients with lower FXYD5 expression (Fig. 1B). Taken together, FXYD5 was substantially elevated in GBM and negatively related to the prognosis of the patients with GBM.

Subsequently, the functional roles of FXYD5 in GBM were examined. After knocking down the FXYD5 in GBM cell lines through RNA interference, the knockdown efficiency was

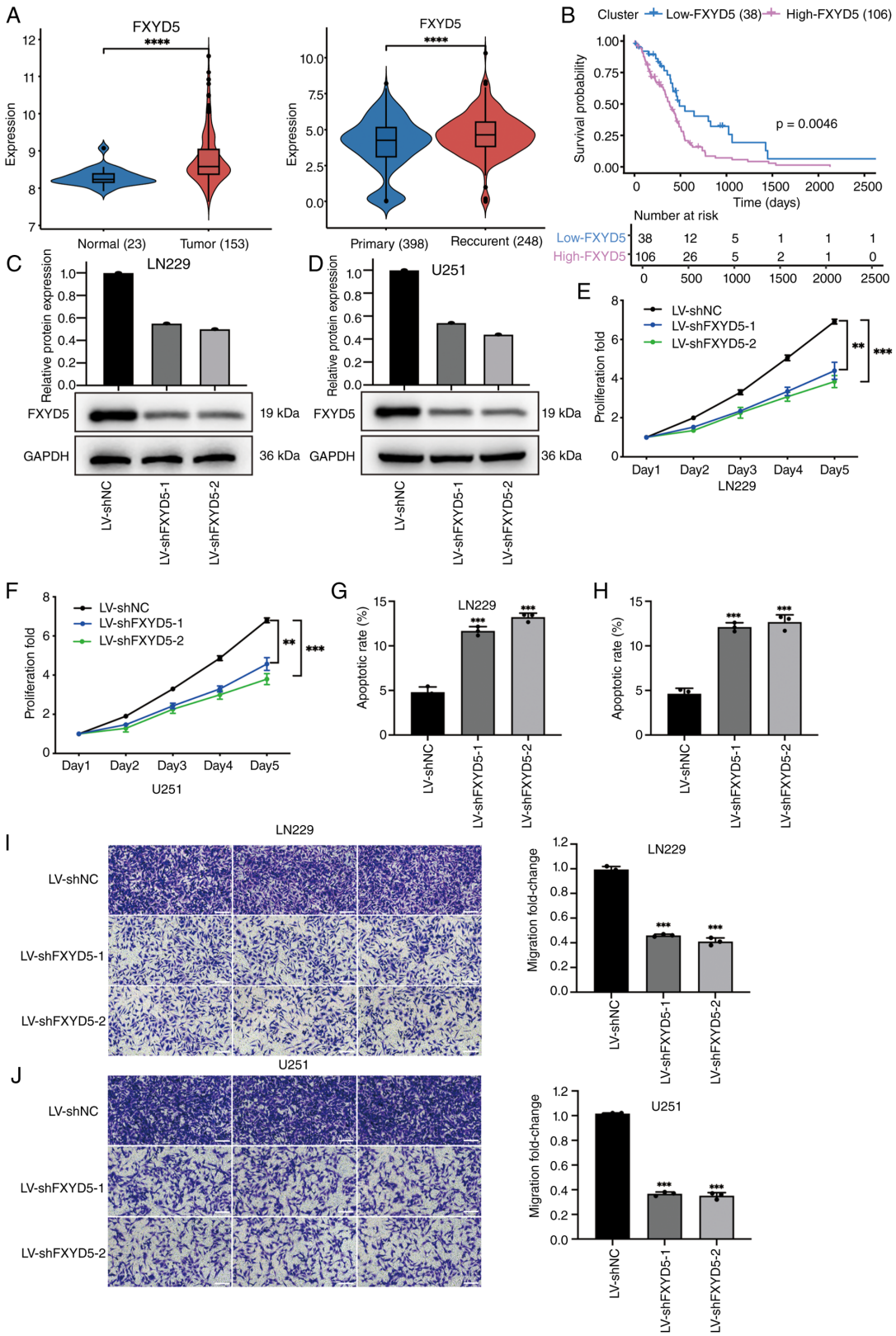

Figure 1. FXYD5 is upregulated in GBM with the prognosis of patients and promotes GBM cell proliferation *in vitro*. (A) Analysis of FXYD5 mRNA expression in 153 GBM samples and 23 normal brain tissue samples in GBM using the GSE4290 dataset (left). Analysis of FXYD5 mRNA expression in 398 primary patient samples and 248 recurrent patient samples in glioma using the China Glioma Genome Atlas-mRNAseq_693 dataset (right). (B) Kaplan-Meier survival curves for overall survival comparing the 38 low-FXYD5 and 106 high-FXYD5 samples within the The Cancer Genome Atlas-GBM dataset. (C and D) Western blot analysis of FXYD5 protein expression following FXYD5 knockdown in (C) LN229 and (D) U251 cells. Below is the bar graph obtained after quantification of protein bands. (E and F) Cell Counting Kit-8 assay examined the relative cell proliferation of (E) LN229 and (F) U251 cells after FXYD5 knockdown. The proliferation fold is the ratio of the OD450 value to that of the first day. (G and H) Flow cytometry examined the apoptotic rate (%) of (G) LN229 and (H) U251 cells after FXYD5 knockdown. The bar chart shows the proportion of early apoptosis combined with late apoptosis. (I and J) Transwell assays demonstrated the inhibition of migratory and invasive capabilities in (I) LN229 and (J) U251 cells with FXYD5 knockdown. Scale bars, 50 μm. The cell counts were quantified using ImageJ software. **P<0.01, ***P<0.001 and ****P<0.0001. GBM, glioblastoma; LV, lentivirus; sh-, short hairpin; NC, negative control.

obvious, and the proliferation of GBM cells, both the LN229 cell line and the U251 cell line, were impaired observably, with an increasing level of apoptosis (Figs. S1C-E; and 1C-H). The Transwell assay also indicated that FXYD5 knockdown could inhibit invasion of GBM cells (Fig. 1I and J). Therefore, the expression of FXYD5 is closely related to growth and invasion in GBM and could be the potential therapeutic target of GBM.

FXYD5 enhances the expression of ACSL4 to promote lipid metabolism in GBM cells. To investigate the role of FXYD5 in the growth of GBM, the mRNAs from high-FXYDH expression and low-FXYDH expression clusters were analyzed. Then, focus was addressed on the 867 upregulating differently expressed genes to GO analysis and it was found that these were significantly enriched in several pathways including phospholipid metabolic process, glycerolipid metabolic process, sphingolipid metabolic process, and lipid transport process (Fig. 2A). It has been reported that GBM cells exhibit enhanced glycolysis, glutamine degradation, lipid and cholesterol synthesis, as well as mitochondrial remodeling (26). A recent study has reported that CDKN2A deletion altered the GBM lipidome and resulted in large changes in lipid metabolic programming in GBM (27). The ssGSEA Score assay also showed significant differences in lipid metabolism levels between the FXYD5-high and FXYD5-low expression groups (Fig. 2B). Then the distribution of lipid metabolism-related gene expression was compared between FXYD5-low or -high clusters (Fig. 2C), finding that the 13 upregulation genes indicate that most of the upregulated genes are mainly concentrated on the process of lipid synthesis. Therefore, it was hypothesized that FXYD5 may mainly promote lipid metabolic reprogramming through lipid synthesis. Besides, lipid metabolism-related genes ACSL4, GPAT3 and SOAT1 were significantly positively correlated with FXYD5 expression (Fig. S1F). GPAT3 is a crucial acyltransferase in the glycerol phosphate pathway, and its downstream metabolites, triacylglycerol and lysophosphatidic acid, were crucial components for the formation of lipid droplets (28). SOAT1 could synthesize cholesterol esters in the endoplasmic reticulum from cholesterol, which was the first step in the process of lipid droplet formation (29). ACSL4 was an enzyme that esterifies CoA into specific polyunsaturated fatty acids, which were essential regulators of fatty acid metabolism (16).

The significance of the lipid metabolism regulation in tumor growth and metastasis has been established in previous studies. It has been confirmed that lipid metabolism has emerged as necessary for GBM development (27,30-32). Therefore, the present investigation focused on examining how FXYD5 promotes GBM development by regulating lipid metabolism in GBM cells. Through lipid assay and Nile red indicator assay, it was demonstrated that the level of fatty acid concentration (Figs. 2D and S1G), intracellular lipid titer (Figs. 2E and S1H), TC content and TG content (Figs. 2F and S1I) were all significantly decreased after FXYD5 knockdown in GBM cells. Moreover, the mRNA (Figs. 2G and S1J) and protein (Figs. 2H and S1K) expression of lipid metabolism key genes ACSL4, GPAT3 and SOAT1 in GBM cells all decreased after FXYD5 knockdown. These results indicated that FXYD5 plays an important role in GBM development by regulating lipid metabolism. Furthermore, FXYD5 could promote the transcription and translation levels of lipid metabolism-related factors, ACSL4, GPAT3 and SOAT1.

FXYD5 promotes lipid metabolism in GBM cells by regulating ACSL4 expression. Previous research has established the significance of ACSL4 control of fatty lipid metabolism in tumor development and metastasis (16,33). To explore the regulatory relationship between FXYD5 and ACSL4, FXYD5 overexpression was performed in ACSL4-knockdown GBM cells. The western blot results indicated that there was a favorable level of overexpression of FXYD5 and knockdown of ACSL4 in both LN229 and U251 cells (Fig. S2A and B). The results demonstrated that overexpression of FXYD5 in GBM cells could restore the mRNA and protein expression levels of ACSL4 that were reduced by ACSL4 knockdown, without influencing FXYD5 expression (Figs. 3A and B; S2C-E). The aforementioned results indicated that FXYD5 is the upstream factor of ACSL4 and could regulate the transcription and translation of ACSL4. Moreover, overexpression of FXYD5 in GBM cells could also restore the level of fatty acid concentration (Figs. 3C and S2F), intracellular lipid titer (Figs. 3D and S2G), TC content and TG content (Figs. 3E and S2H) in GBM cells that were reduced by ACSL4 knockdown. These findings confirmed the notion that FXYD5 advanced the intracellular lipid metabolism hinged on its regulation of ACSL4 expression.

Moreover, overexpression of ACSL4 was performed in LN229 cells that had been knocked down for FXYD5 and it was found that overexpression of ACSL4 was unable to significantly restore the decreased mRNA and protein levels of FXYD5 (Figs. 3F and G; S2I and J), nor could it restore the decreased level of fatty acid concentration (Fig. 3H), intracellular lipid titer (Fig. 3I), and TC content and TG content (Fig. 3J) caused by the knockdown of FXYD5. The aforementioned results further confirmed that FXYD5 acted as an upstream regulatory factor for ACSL4 and regulates the lipid metabolism of GBM cells.

FXYD5 regulates ACSL4 via activating the PI3K/AKT signaling pathway, promoting GBM growth and invasion. After analyzing the Kyoto Encyclopedia of Genes and Genomes (KEGG), it was found that the PI3K/AKT signaling pathway was also significantly enriched (Fig. 4A). The ssGSEA Score assay showed significant differences in the PI3K/AKT signal pathway between the FXYD5-high and FXYD5-low expression groups (Figs. 4B and S3A). A previous study has confirmed that the typical molecular changes in GBM include mutations in genes regulating PI3K signaling (4). The PI3K/AKT signaling pathway has been confirmed to be the targeted therapy for GBM (34-36). However, there have been no studies examining a regulatory relationship between FXYD5 and the PI3K/AKT pathway. Western blot analysis confirmed decreased expression of phosphorylated (p-) PI3K and AKT following FXYD5 knockdown in GBM cells, demonstrating that FXYD5 could regulate the PI3K/AKT pathway (Figs. 4C; S3B and C). To investigate the relationship between FXYD5 and PI3K, immunoprecipitation (IP) was performed using the endogenous antibody of FXYD5 in FXYD5-overexpressing U251 and LN229 cells. The western blot showed that no PI3K-p85 and PI3K-p110α were detected in the IP products (Fig. S3D). The results indicated that FXYD5 did not physically bind to

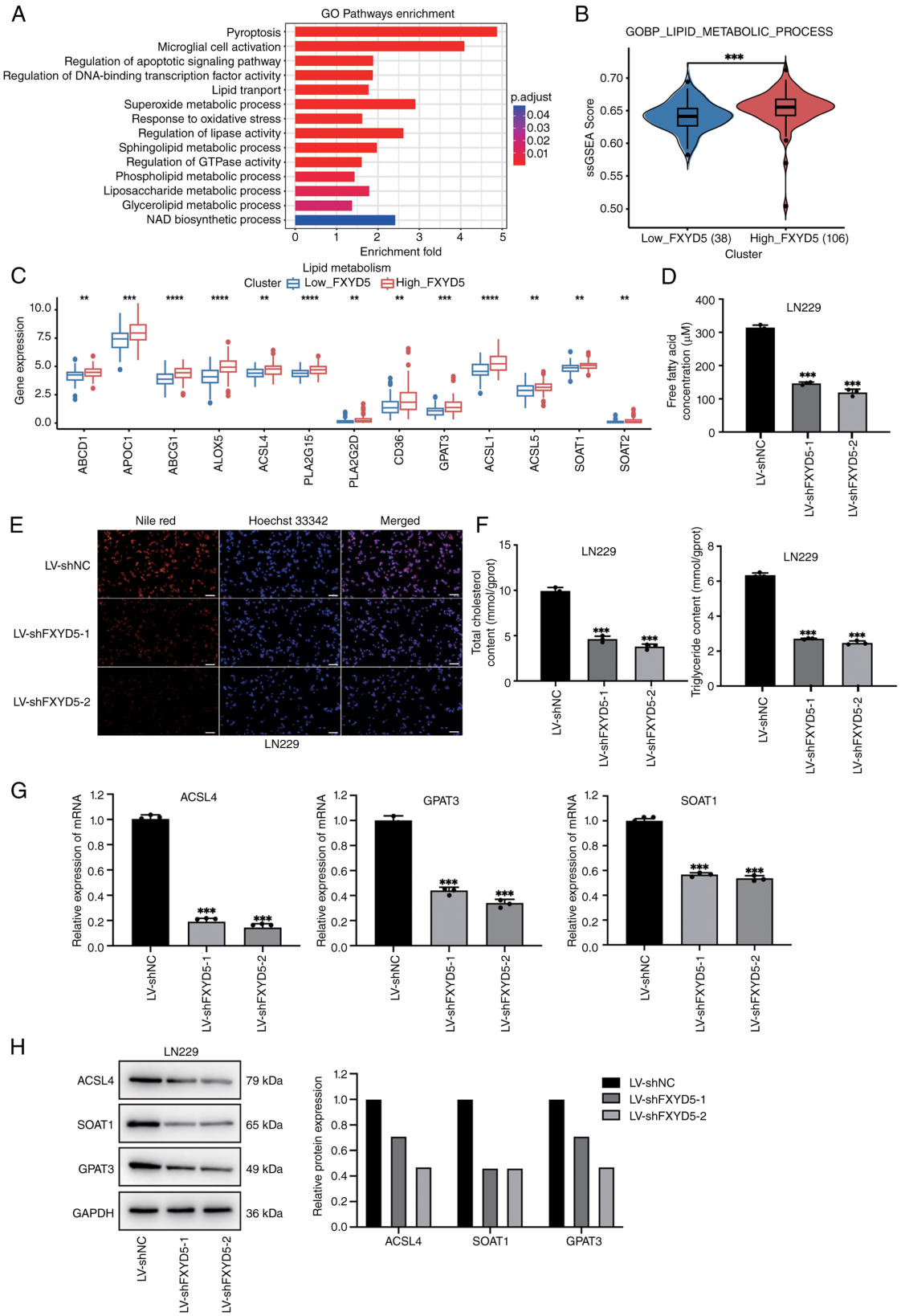

Figure 2. FXYD5 promotes GBM tumor development by upregulating lipid metabolism. (A) The GO analysis of the differentially expressed genes between 38 FXYD5-low or 106 FXYD5-high clusters using the The Cancer Genome Atlas-GBM dataset. (B) ssGSEA Score of Lipid metabolic pathway between 38 FXYD5-low or 106 FXYD5-high clusters. (C) Comparison of the distribution of Lipid metabolism-related genes expression between 38 FXYD5-low or 106 FXYD5-high clusters, showing 13 upregulation genes. (D) Level of free fatty acid concentration of LN229 cells after FXYD5 knockdown. (E) Nile Red indicator assay evaluating the effect of FXYD5 knockdown on intracellular lipid titer in LN229 cells. Red fluorescence representing lipid droplets, while blue fluorescence representing the cell nucleus. Scale bars, 500 μm. (F) Level of total cholesterol content and triglyceride content of LN229 cells after FXYD5 knockdown. (G) mRNA expression of lipid metabolism key genes, ACSL4, GPAT3 and SOAT1 in LN229 cells after FXYD5 knockdown. (H) Western blot analysis of ACSL4, GPAT3 and SOAT1 protein expression in LN229 cells after FXYD5 knockdown. The bar graph obtained after quantification of protein bands is in right. **P<0.01, ***P<0.001 and ****P<0.0001. GBM, glioblastoma; GO, Gene Ontology; SOAT1, sterol O-acyltransferase 1; ACSL4, long-chain acyl-coenzyme A (CoA) synthase 4; GPAT3, glycerol-3-phosphate acyltransferase 3; LV, lentivirus; sh-, short hairpin; NC, negative control.

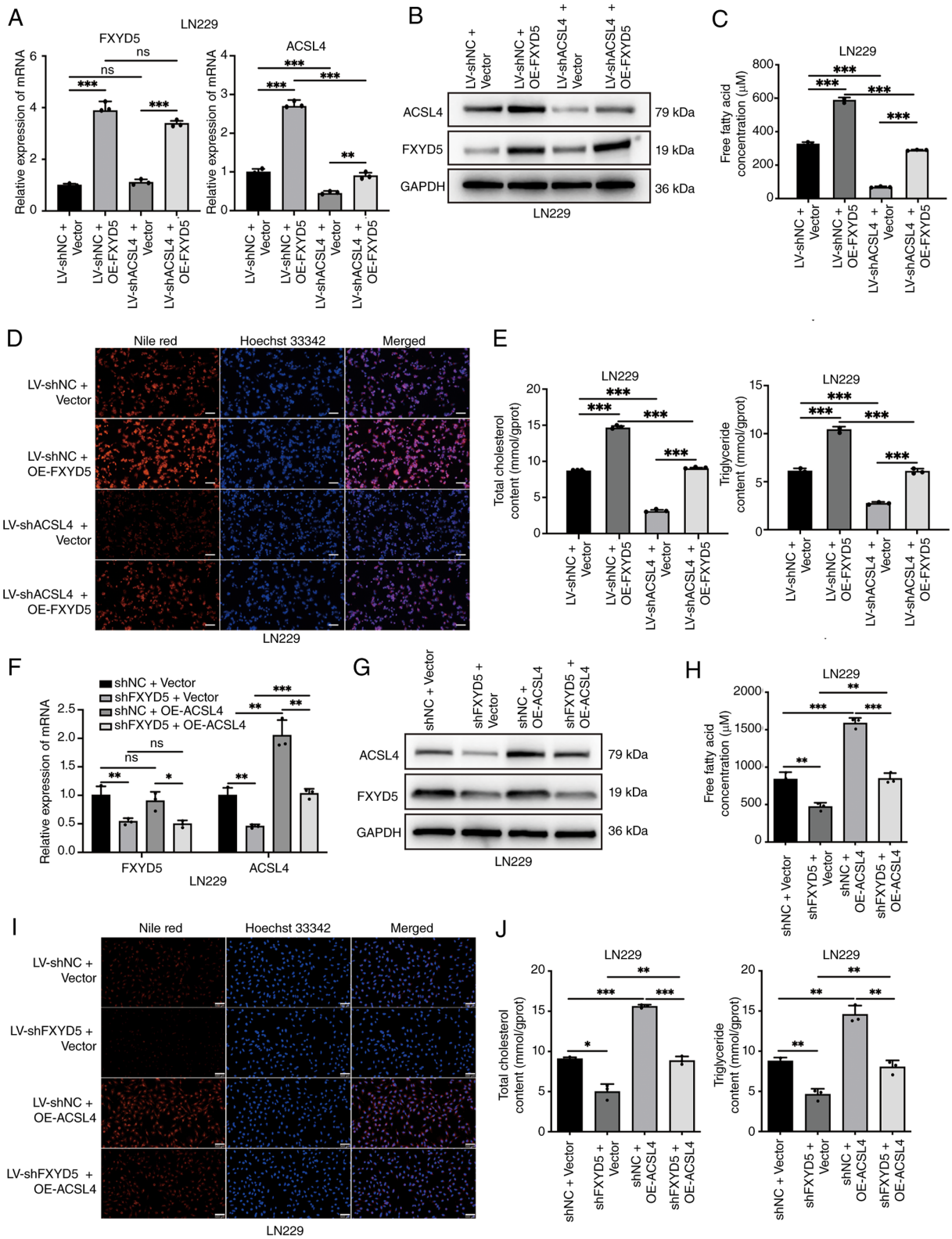

Figure 3. FXYD5 affects intracellular lipid metabolism in glioblastoma cells via ACSL4 factor. (A) mRNA expression of FXYD5 and ACSL4 in LN229 cells after overexpression of FXYD5 and knockdown of ACSL4. (B) Western blot analysis of FXYD5 and ACSL4 protein expression in LN229 cells after overexpression of FXYD5 and knockdown of ACSL4. (C) Level of free fatty acid concentration of LN229 cells after overexpression of FXYD5 and knockdown of ACSL4. (D) Nile Red indicator assay evaluating the effect of overexpression of FXYD5 and knockdown of ACSL4 on intracellular lipid titer in LN229 cells. Scale bars, 500 μm. (E) Level of total cholesterol content and triglyceride content of LN229 cells after overexpression of FXYD5 and knockdown of ACSL4. (F) mRNA expression of FXYD5 and ACSL4 in LN229 cells after knockdown of FXYD5 and overexpression of ACSL4. (G) Western blot analysis of FXYD5 and ACSL4 protein expression in LN229 cells after knockdown of FXYD5 and overexpression of ACSL4. (H) Level of free fatty acid concentration of LN229 cells after knockdown of FXYD5 and overexpression of ACSL4. (I) Nile Red indicator assay evaluating the effect of knockdown of FXYD5 and overexpression of ACSL4 on intracellular lipid titer in LN229 cells. Scale bars, 500 μm. Red fluorescence representing lipid droplets, while blue fluorescence representing the cell nucleus. (J) Level of total cholesterol content and triglyceride content of LN229 cells after knockdown of FXYD5 and overexpression of ACSL4. *P<0.05, **P<0.01 and ***P<0.001. ACSL4, long-chain acyl-coenzyme A (CoA) synthase 4; LV, lentivirus; sh-, short hairpin; NC, negative control; OE, overexpression; ns, not significant.

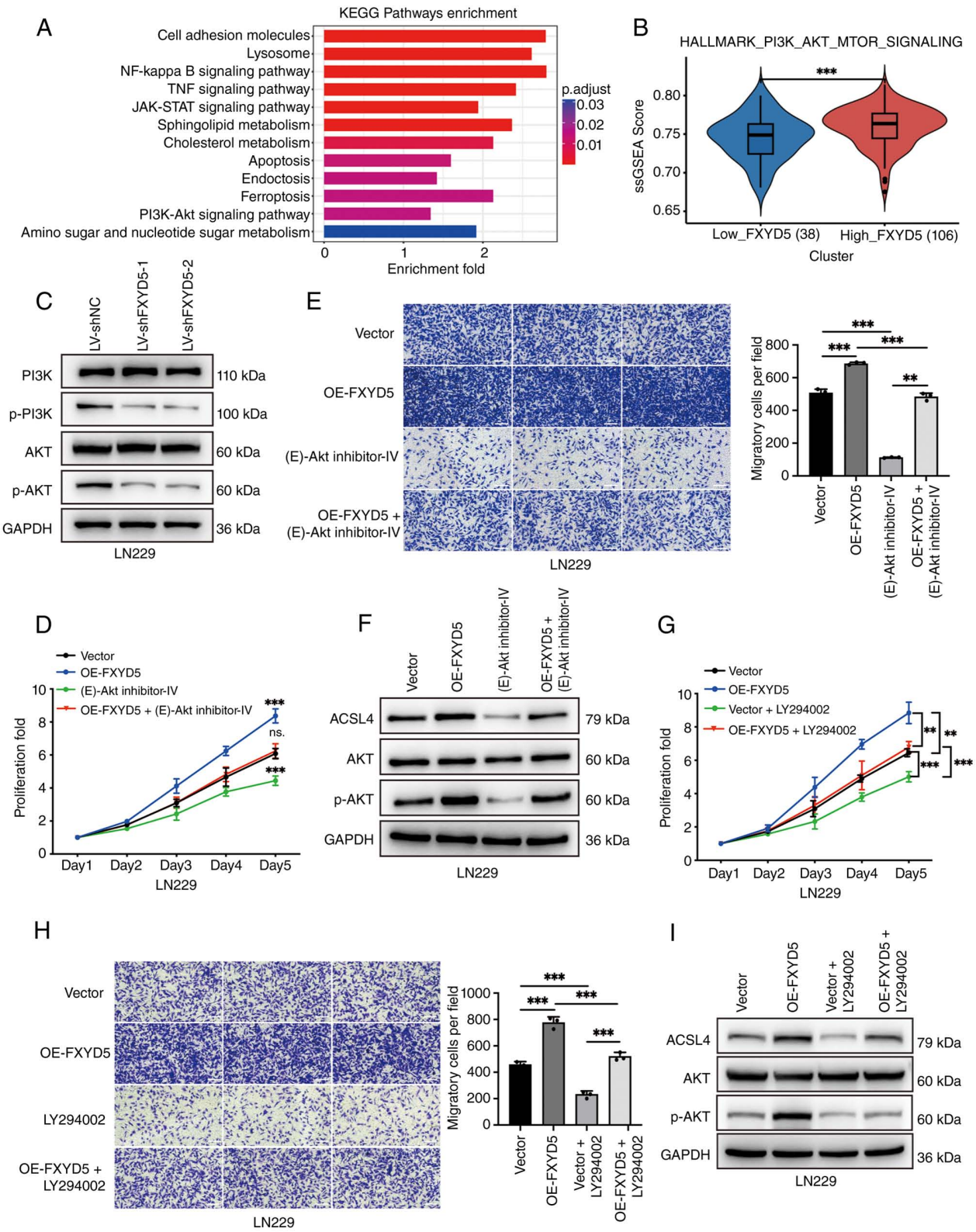

Figure 4. FXYD5 promotes GBM tumor development by upregulating lipid metabolism through the PI3K/AKT/ACSL4 signaling pathway. (A) The KEGG analysis of the differentially expressed genes between 38 FXYD5-low or 106 FXYD5-high clusters using The Cancer Genome Atlas-GBM dataset. (B) ssGSEA Score of PI3K/AKT pathway between 38 FXYD5-low or 106 FXYD5-high clusters. (C) Western blot analysis of PI3K, AKT, p-PI3K and p-AKT protein expression in LN229 cells after FXYD5 knockdown. (D) Cell Counting Kit-8 assay examined the relative cell proliferation of LN229 cells after overexpression of FXYD5 and using AKT inhibitor (E)-Akt inhibitor-IV. (E) Transwell assays demonstrated the inhibition of migratory and invasive capabilities in LN229 cells after overexpression of FXYD5 and using AKT inhibitor (E)-Akt inhibitor-IV. (F) Western blot analysis of AKT, p-AKT and ACSL4 protein expression in LN229 cells after overexpression of FXYD5 and using AKT inhibitor (E)-Akt inhibitor-IV. (G) Cell Counting Kit-8 assay examined the relative cell proliferation of LN229 cells after overexpression of FXYD5 and using PI3K inhibitor LY294002. (H) Transwell assays demonstrated the inhibition of migratory and invasive capabilities in LN229 cells after overexpression of FXYD5 and using PI3K inhibitor LY294002. Scale bars, 50 μm. (I) Western blot analysis of AKT, p-AKT and ACSL4 protein expression in LN229 cells after overexpression of FXYD5 and using PI3K inhibitor LY294002. **P<0.01 and ***P<0.001. GBM, glioblastoma; KEGG, Kyoto Encyclopedia of Genes and Genomes; LV, lentivirus; sh-, short hairpin; NC, negative control; OE, overexpression; ns, not significant.

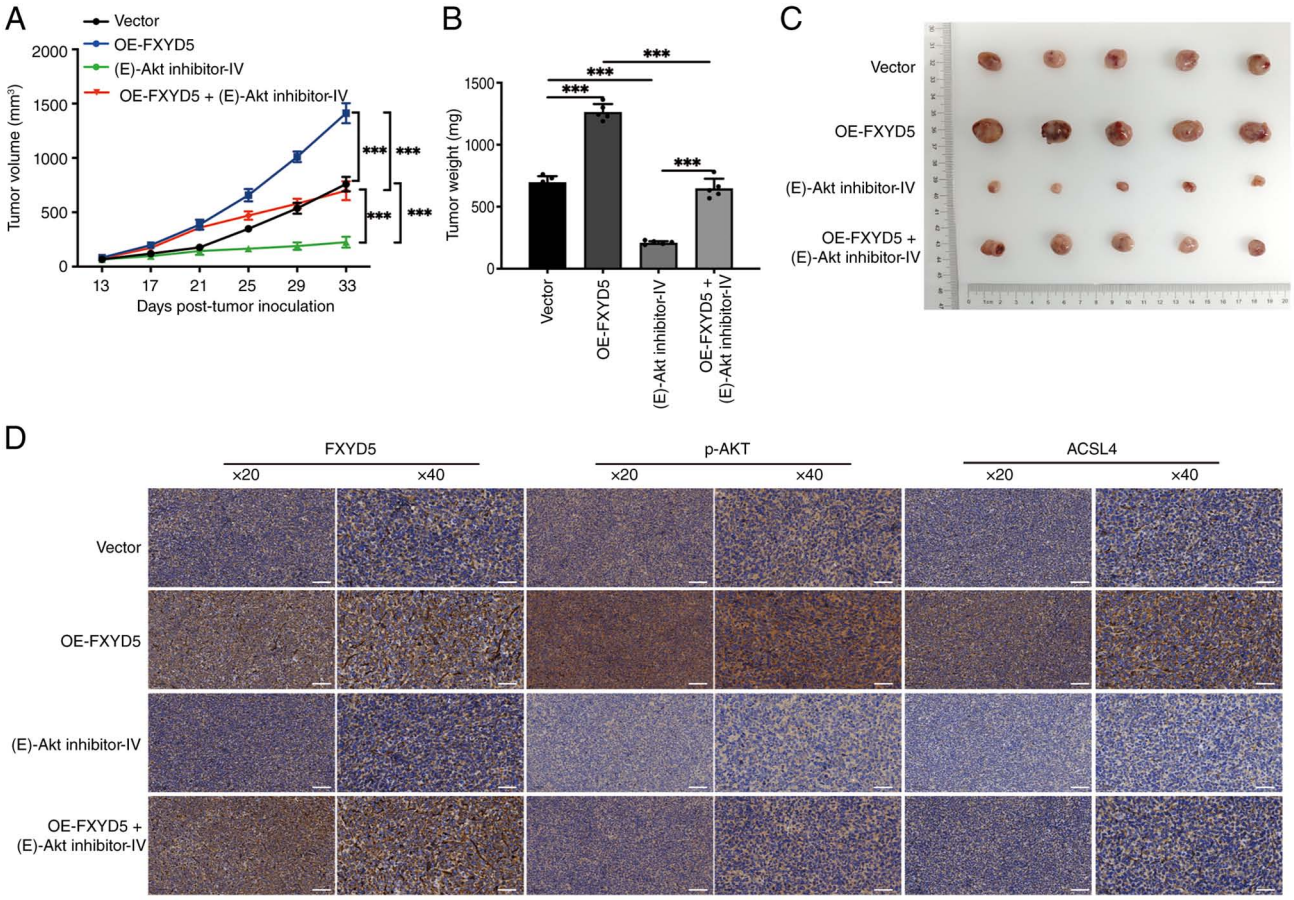

Figure 5. PI3K/AKT inhibitors have an inhibitory effect on GBM tumor development induced by overexpression of FXYD5 *in vivo*. (A-D) LN229 cell-derived xenograft experiment in 20 male BALB/c nude mice, randomized into four groups (Vector group, OE-FXYD5 group, AKT inhibitor group and OE-FXYD5 group + AKT inhibitor group) under a double-blind protocol (n=5 per group), (E)-Akt inhibitor-IV (100 μmol/kg) was injected subcutaneously on the 21st, 25th and 29th days after the GBM cells were inoculated. Vector group was treated with PBS accordingly. (A) Tumor volume by subcutaneous injection of LN229 cells. (B) Tumor weight by subcutaneous injection of LN229 cells. (C) Representative image of a subcutaneous tumor in a mouse model. (D) Immunohistochemical analysis of FXYD5, p-AKT, and ACSL4 in subcutaneous xenograft tumors from Vector group, OE-FXYD5 group, AKT inhibitor group, and OE-FXYD5 group + AKT inhibitor group. Montage scale bar, 100 μm. ***P<0.001. GBM, glioblastoma; OE, overexpression; ACSL4, long-chain acyl-coenzyme A (CoA) synthase 4; p-, phosphorylated.

either the catalytic subunit or the regulatory subunit of PI3K. FXYD5 may be achieved through an indirect mechanism to activate the PI3K/AKT pathway.

Furthermore, overexpression of FXYD5 in GBM cells could restore the proliferation and invasion of GBM cells that were treated by the AKT inhibitor (E)-Akt inhibitor-IV (Figs. 4D and E; S3E and F), revealing that FXYD5 could potentially enhance the development of GBM by activating the PI3K/AKT pathway and FXYD5 was the upstream factor of the PI3K/AKT pathway. Western blot analysis indicated that overexpressing FXYD5 could restore the protein expression of ACSL4 in GBM cells that were treated by the AKT inhibitor (E)-AKT inhibitor-IV (Figs. 4F; S3G and H). Besides, another PI3K inhibitor, LY294002, was used and it found that FXYD5 overexpression could similarly restore the proliferation and invasion of GBM cells, and the protein expression of ACSL4 in GBM cells treated by LY294002 (Figs. 4G-I; S4A). Similarly, knockdown of FXYD5 could inhibit the proliferation and invasion of GBM cells induced by the overexpression of PIK3CA-H1047R, a carcinogenic mutation located on the catalytic subunit PI3K p110α, which could enhance the PI3K signal (Fig. S3B and C). In conclusion, the findings suggested that targeting FXYD5 leads to decreased growth of GBM by suppressing the PI3K/AKT signaling pathway-mediated expression of ACSL4, then decreasing the lipid metabolism level in GBM cells.

PI3K/AKT inhibitor-treated GBM is induced by FXYD5 overexpression in vivo. Some studies have reported that certain targets could activate the PI3K/AKT pathway, improving glioma or GBM growth *in vivo* (37,38). However, no study has yet demonstrated that FXYD5 could promote the development of GBM through the PI3K/AKT pathway *in vivo*.

To evaluate the therapeutic impact of FXYD5 on GBM *in vivo*, FXYD5 overexpressed-LN229 cells were subcutaneously injected in a murine model. Tumor size was measured starting 13 days after subcutaneous injection, and the PI3K/AKT pathway inhibitor treatment group was able to inhibit tumor growth promoted by FXYD5 overexpression (Fig. 5A). The final tumor size and weight of mice in the PI3K/AKT inhibitor treatment group were significantly smaller than those of mice in the FXYD5 overexpression group alone (Fig. 5B and C). As expected, it was identified that the PI3K/AKT inhibitor prevented tumor development induced by FXYD5, which was

further supported by IHC staining and analysis (Fig. 5D). IHC staining showed that the p-AKT and ACSL4 were obviously increased in the FXYD5-overexpressed group. Also, using a PI3K/AKT inhibitor could prevent the increased p-AKT and ACSL4 induced by FXYD5 overexpression. The NC ruled out the possibility of false positive antibodies (Fig. S4D). In final analysis, the findings suggested that targeting FXYD5 leads to decreased progression of GBM *in vivo* via the PI3K/AKT/ACSL4 pathway.

Discussion

GBM is a highly malignant neoplasm of the central nervous system with a short survival period, which is distinguished by rapid growth, widespread infiltration and resistance to therapies (39). GBM is usually treated with chemotherapy and radiotherapy (40,41). However, issues, such as chemoresistance and radioresistance, still need to be addressed. The complexity and heterogeneity of GBM have long hampered therapeutic progress, but modern technologies, such as single-cell and spatially resolved transcriptomics, are offering a new way to investigate these complicated malignancies (42). TCGA presented a study examining the main mutation in GBM, according to which three major genetic events occur in GBM: RTK gene amplification and mutational activation, PI3K pathway activation, and p53 and retinoblastoma tumor suppressor pathway inactivation (43). It has been demonstrated that targeting certain signaling pathways, such as the NF-κB signaling pathway, the Wnt pathway and the PI3K/AKT/mTOR signaling pathway, could prevent the development of GBM (44). Therefore, novel gene-based targeted therapies for GBM are urgently needed.

Several studies have documented the involvement of FXYD5 in the progression of various cancers (45,46), except GBM. In the present study, analysis of public databases suggested a positive correlation between the expression of FXYD5 in GBM tissue samples from clinical cases. Besides, it was found that knockdown of FXYD5 could increase the level of GBM cell apoptosis, suppressing the proliferation and migration of GBM cells. Nevertheless, further research is needed to elucidate the exact role of FXYD5 in promoting growth and invasion in GBM.

Results of bioinformatics analysis showed that lipid metabolism-related pathways were enriched in FXYD5 clusters, and FXYD5 was significantly positively correlated with lipid metabolism-related factors ACSL4, GPAT3 and SOAT1. Subsequently, it was confirmed that knocking down FXYD5 indeed could reduce the level of fatty acid concentration, intracellular lipid titer, TC content and TG content in GBM cells. ACSL4, an essential regulator of fatty acid metabolism, might be a potential therapeutic target for tumor (16). Knockdown of FXYD5 could inhibit the transcription and translation of ACSL4. Furthermore, overexpression of FXYD5 could similarly restore the decreased lipid metabolism level caused by ACSL4-knockdown. However, overexpression of ACSL4 was unable to significantly restore the decreased lipid metabolism level caused by the knockdown of FXYD5. These demonstrated that FXYD5, as the upstream factor of ACSL4, could influence the lipid metabolism level of GBM cells by regulating the gene expression of ACSL4.

Targeting PI3K/AKT signaling pathway was a successful therapeutic strategy in GBM (31). A previous study reported that activation of PI3K/AKT signaling leads to the stemness of GBM cells increases (47). Antitumor agents have been found to induce both apoptosis and autophagy in GBM via affecting the PI3K/AKT/mTOR axis. Sinomenine ester derivative, a suppressor of GBM progression, was revealed to inhibit the PI3K/AKT/mTOR pathway to induce apoptosis and autophagy via the mitochondrial pathway in reducing GBM progression (48). Punicic acid, another anticancer agent, was utilized in inducing apoptosis and decreasing metastasis of GBM cells by suppressing the PI3K/AKT/mTOR axis (49-51). Bioinformatics investigation also revealed the connection between FXYD5 and the PI3K/AKT pathway. It was found that knockdown of FXYD5 could inhibit the activation of the PI3K/AKT pathway. Moreover, the PI3K/AKT inhibitor similarly restored the proliferation and migration of GBM cells and increased expression of ACSL4 caused by overexpression of FXYD5, which demonstrated that FXYD5 could affect the transcription and translation of ACSL4 via the PI3K/AKT pathway, thus influencing the progression of GBM. However, using the FXYD5 antibody could not immunoprecipitate the protein of PI3K-p85 and PI3K-p110α, indicating that FXYD5 did not interact with either the catalytic subunit or the regulatory subunit of PI3K and may activate PI3K/AKT through an indirect mechanism, which should be further explored in future research. In conclusion, the present study elucidated the role of the FXYD5/PI3K/AKT/ACSL4 signaling pathway in facilitating development and invasion in GBM.

However, the present study still has several limitations. In the present experiment, the GBM cell lines LN229 and U251 were used as the model cells. A study has shown that tumor stem cells derived from GBMs cultured in bFGF and EGF more closely mirror the phenotype and genotype of primary tumors than do serum-cultured cell lines (52). Tumor stem cells derived from GBM that have been cultured with bFGF and EGF could be selected as the cell model for experimental research in future studies. Several limitations in the present bioinformatic analyses should be acknowledged. The prognostic cutoff value, survival analysis and pathway predictions (GO, KEGG and ssGSEA) were derived solely from the TCGA-GBM dataset and were not independently validated in a separate computational cohort. However, the upregulation of FXYD5 in GBM and its associations with higher tumor grade and recurrence were validated across multiple independent datasets (GSE4290 and CGGA-mRNAseq_693). The predicted pathways were subsequently supported by extensive *in vitro* and *in vivo* functional experiments. Future studies using additional GBM cohorts, such as CGGA survival data or institutional clinical samples, will be necessary to confirm the prognostic value of FXYD5 and to independently validate these bioinformatic predictions. Furthermore, it has been shown by the authors that FXYD5 does not directly target PI3K, but the specific indirect way through which it activates the PI3K/AKT pathway has not yet identified (53). FXYD5 has been reported to function as a regulator of ion transport, particularly by modulating Na^+,K^+-ATPase activity. Changes in ion transport can affect membrane potential, ion homeostasis and downstream signaling cascades. Emerging evidence indicates that alterations in ion homeostasis can influence various

signaling pathways, including PI3K/AKT (54). Therefore, it is plausible that FXYD5 indirectly activates PI3K/AKT signaling by modifying the cellular ionic environment or membrane potential. In future studies, it is planned to explore this possibility by examining the effects of FXYD5 expression on intracellular sodium and potassium concentrations, as well as on membrane potential. Besides, both orthotopic intracranial injection models and subcutaneous injection models are currently utilized in mouse experiments for GBM. However, the orthotopic intracranial model preserved the brain-specific microenvironment and demonstrated greater clinical relevance, consequently being more widely adopted. The authors' xenograft studies are only conducted subcutaneously, which is used as a preliminary *in vivo* model because it allows easier tumor monitoring, repeated treatment administration, and assessment of FXYD5-dependent tumor growth. However, the limitation should also mention that the model does not reproduce the blood-brain barrier, intracranial pressure constraints, or the neural tumor microenvironment. The clinical implications are hindered by the lack of a brain microenvironment. In the later stage, further experiments will be conducted using orthotopic intracranial injection models. Thus, the results of such experiments would be more reliable and meaningful for preclinical and translational GBM research.

In summary, the present study identified that FXYD5 was a potential therapeutic target in GBM. The research findings indicate that the FXYD5 could trigger the activation of the PI3K/AKT signaling pathway. The expression of FXYD5 led to the activation of the PI3K/AKT signaling pathway, subsequently enhancing the expression of lipid metabolism-related factor ACSL4, advancing lipid metabolism, thereby facilitating GBM tumor development and invasion. Targeting FXYD5 could inhibit the activation of the PI3K/AKT pathway, which decreased the expression of lipid metabolism-related gene ACSL4, then preventing lipid metabolism in GBM cells. The FXYD5/PI3K/AKT/ACSL4 signaling cascade is significantly involved in treating GBM. These results suggested that targeting this signaling cascade may hold promise as a therapeutic strategy for GBM.

Acknowledgements

Not applicable.

Funding

No funding was received.

Availability of data and materials

The data generated in the present study may be requested from the corresponding author.

Authors' contributions

BW, YQ and HC performed the experiments, wrote the manuscript and analyzed the data. YZ and LJ helped analyze the data. XH designed and supervised the study. BW and YQ confirm the authenticity of all the raw data All authors read and approved the final version of the manuscript.

Ethics approval and consent to participate

The present study was conducted in accordance with relevant guidelines and regulations. For animal experiments, approval was obtained from the Hubei Provincial Center for Disease Control and Prevention (approval no. 202510218; Wuhan, China).

Patient consent for publication

Not applicable.

Competing interests

The authors declare that they have no competing interests.

References

1. Le Rhun E, Preusser M, Roth P, Reardon DA, van den Bent M, Wen P, Reifenberger G and Weller M: Molecular targeted therapy of glioblastoma. Cancer Treat Rev 80: 101896, 2019.
2. Weller M, Wick W, Aldape K, Brada M, Berger M, Pfister SM Nishikawa R, Rosenthal M, Wen PY, Stupp R and Reifenberger G: Glioma. Nat Rev Dis Primers 1: 15017, 2015.
3. Barnholtz-Sloan JS, Ostrom QT and Cote D: Epidemiology of brain tumors. Neurol Clin 36: 395-419, 2018.
4. Wirsching HG, Galanis E and Weller M: Glioblastoma. Handb Clin Neurol 134: 381-397, 2016.
5. Gilbert MR, Wang M, Aldape KD, Stupp R, Hegi ME, Jaeckle KA Armstrong TS, Wefel JS, Won M and Blumenthal DT: Dose-dense temozolomide for newly diagnosed glioblastoma: A randomized phase III clinical trial. J Clin Oncol 31: 4085-4091, 2013.
6. Tan AC, Ashley DM, López GY, Malinzak M, Friedman HS and Khasraw M: Management of glioblastoma: State of the art and future directions. CA Cancer J Clin 70: 299-312, 2020.
7. Rocha Pinheiro SL, Lemos FFB, Marques HS, Silva Luz M, de Oliveira Silva LG, Faria Souza Mendes Dos Santos C, da Costa Evangelista K, Calmon MS, Sande Loureiro M and Freire de Melo F: Immunotherapy in glioblastoma treatment: Current state and future prospects. World J Clin Oncol 14: 138-159, 2023.
8. Gaiaschi L, Bottone MG and De Luca F: Towards effective treatment of glioblastoma: The role of combination therapies and the potential of phytotherapy and micotherapy. Curr Issues Mol Biol 46: 14324-14350, 2024.
9. Besso MJ, Rosso M, Lapyckyj L, Moiola CP, Matos ML, Mercogliano MF, Schillaci R, Reventos J, Colas E, Gil-Moreno A, *et al*: FXYD5/Dysadherin, a biomarker of endometrial cancer myometrial invasion and aggressiveness: Its relationship With TGF-β1 and NF-κB Pathways. Front Oncol 9: 1306, 2019.
10. Bai Y, Li LD, Li J, Chen RF, Yu HL, Sun HF, Wang JY and Lu X: A FXYD5/TGF-β/SMAD positive feedback loop drives epithelial-to-mesenchymal transition and promotes tumor growth and metastasis in ovarian cancer. Int J Oncol 56: 301-314, 2020.
11. Hotta T, Nariai Y, Kajitani N, Kadota K, Maruyama R, Tajima Y, Isobe T, Kamino H and Urano T: Generation of the novel anti-FXYD5 monoclonal antibody and its application to the diagnosis of pancreatic and lung cancer. Biochimie 208:160-169, 2023.
12. Niinivirta A, Salo T, Åström P, Juurikka K and Risteli M: Prognostic value of dysadherin in cancer: A systematic review and meta-analysis. Front Oncol 12: 945992, 2022.
13. Mao Y, Hu Y, Meng H, Qin J, An Q, Zhang C, Guo C, Zhao Y, Tan D, Ge X and Shi C: FXYD5 regulates gastric cancer cell metastasis and drug resistance by EMT modulation. Cancer Gene Ther 32: 318-326, 2025.
14. Lubarski-Gotliv I, Dey K, Kuznetsov Y, Kalchenco V, Asher C and Garty H: FXYD5 (dysadherin) may mediate metastatic progression through regulation of the β-Na+-K+-ATPase subunit in the 4T1 mouse breast cancer model. Am J Physiol Cell Physiol 313: C108-C117, 2017.
15. Juurikka K, Dufour A, Pehkonen K, Mainoli B, Campioni Rodrigues P, Solis N, Klein T, Nyberg P, Overall CM, Salo T and Åström P: MMP8 increases tongue carcinoma cell-cell adhesion and diminishes migration via cleavage of anti-adhesive FXYD5. Oncogenesis 10: 44, 2021.

16. Ding K, Liu C, Li L, Yang M, Jiang N, Luo S and Sun L: Acyl-CoA synthase ACSL4: An essential target in ferroptosis and fatty acid metabolism. Chin Med J (Engl) 136: 2521-2537, 2023.
17. Li YJ, Fahrmann JF, Aftabizadeh M, Zhao Q, Tripathi SC, Zhang C, Yuan Y, Ann D, Hanash S and Yu H: Fatty acid oxidation protects cancer cells from apoptosis by increasing mitochondrial membrane lipids. Cell Rep 39: 110870, 2022.
18. Zhang HL, Hu BX, Li ZL, Du T, Shan JL, Ye ZP, Peng XD, Li X, Huang Y, Zhu XY, *et al*: PKCβII phosphorylates ACSL4 to amplify lipid peroxidation to induce ferroptosis. Nat Cell Biol 24: 88-98, 2022.
19. Wang Y, Hu M, Cao J, Wang F, Han JR, Wu TW Li L, Yu J, Fan Y, Xie G, *et al*: ACSL4 and polyunsaturated lipids support metastatic extravasation and colonization. Cell 188: 412-429.e27, 2025.
20. Livak KJ and Schmittgen TD: Analysis of relative gene expression data using real-time quantitative PCR and the 2(-Delta Delta C(T)) method. Methods 25: 402-408, 2001.
21. Sun L, Hui AM, Su Q, Vortmeyer A, Kotliarov Y, Pastorino S, Passaniti A, Menon J, Walling J, Bailey R, *et al*: Neuronal and glioma-derived stem cell factor induces angiogenesis within the brain. Cancer Cell 9: 287-300, 2006.
22. Zhao Z, Zhang KN, Wang Q, Li G, Zeng F, Zhang Y Wu F, Chai R, Wang Z, Zhang C, *et al*: Chinese glioma genome atlas (CGGA): A comprehensive resource with functional genomic data from Chinese glioma patients. Genomics Proteomics Bioinformatics 19: 1-12, 2021.
23. Love MI, Huber W and Anders S: Moderated estimation of fold change and dispersion for RNA-seq data with DESeq2. Genome Biol 15: 550, 2014.
24. Hänzelmann S, Castelo R and Guinney J: GSVA: Gene set variation analysis for microarray and RNA-seq data. BMC Bioinformatics 14: 7, 2013.
25. Biasiotta A, D'Arcangelo D, Passarelli F, Nicodemi EM and Facchiano A: Ion channels expression and function are strongly modified in solid tumors and vascular malformations. J Transl Med 14: 285, 2016.
26. Chung J, Saad J, Kafri A, Rossignol J, Verbrugge M and Bakke J: Metabolism of glioblastoma: A review of metabolic adaptations and metabolic therapeutic interventions. Front Oncol 15: 712576, 2025.
27. Minami JK, Morrow D, Bayley NA, Fernandez EG, Salinas JJ, Tse C, Zhu H, Su B, Plawat R, Jones A, *et al*: CDKN2A deletion remodels lipid metabolism to prime glioblastoma for ferroptosis. Cancer Cell 41: 1048-1060.e9, 2023.
28. Wang Y, Xu C, Yang X, Liu X, Guo Z, Lin X, Li L and Huang Z: Glycerol-3-phosphate acyltransferase 3-mediated lipid droplets accumulation confers chemoresistance of colorectal cancer. MedComm (2020) 5: e486, 2024.
29. Kou Y, Geng F and Guo D: Lipid metabolism in glioblastoma: From de novo synthesis to storage. Biomedicines 10: 1943, 2022.
30. Lee H, Kim D and Youn B: Targeting oncogenic rewiring of lipid metabolism for glioblastoma treatment. Int J Mol Sci 23: 13818, 2022.
31. Shakya S, Gromovsky AD, Hale JS, Knudsen AM, Prager B, Wallace LC Penalva LOF, Brown HA, Kristensen BW, Rich JN, *et al*: Altered lipid metabolism marks glioblastoma stem and non-stem cells in separate tumor niches. Acta Neuropathol Commun 9: 101, 2021.
32. Broadfield LA, Pane AA, Talebi A, Swinnen JV and Fendt SM: Lipid metabolism in cancer: New perspectives and emerging mechanisms. Dev Cell 56: 1363-1393, 2021.
33. Lei Z, Luo Y, Lu J, Fu Q, Wang C, Chen Q Zhang Z and Zhang L: FBXO22 promotes HCC angiogenesis and metastasis via RPS5/AKT/HIF-1α/VEGF-A signaling axis. Cancer Gene Ther 32: 198-213, 2025.
34. Li X, Wu C, Chen N, Gu H, Yen A, Cao L, Wang E and Wang L: PI3K/Akt/mTOR signaling pathway and targeted therapy for glioblastoma. Oncotarget 7: 33440-33450, 2016.
35. Barzegar Behrooz A, Talaie Z, Jusheghani F, Łos MJ, Klonisch T and Ghavami S: Wnt and PI3K/Akt/mTOR survival pathways as therapeutic targets in glioblastoma. Int J Mol Sci 23: 1353, 2022.
36. Hashemi M, Etemad S, Rezaei S, Ziaolhagh S, Rajabi R, Rahmanian P, Abdi S, Koohpar ZK, Rafiei R, Raei B, *et al*: Progress in targeting PTEN/PI3K/Akt axis in glioblastoma therapy: Revisiting molecular interactions. Biomed Pharmacother 158: 114204, 2023.
37. Zhang D, Wang X, Wang X, Wang Z, Ma S, Zhang C, Li S and Jia W: CPNE3 regulates the cell proliferation and apoptosis in human Glioblastoma via the activation of PI3K/AKT signaling pathway. J Cancer 12: 7277-7286, 2021.
38. Zhang A, Peng S, Sun S, Ye S, Zhao Y and Wu Q: NRBP1 promotes malignant phenotypes of glioblastoma by regulating PI3K/Akt activation. Cancer Med 13: e70100, 2024.
39. Yabo YA and Heiland DH: Understanding glioblastoma at the single-cell level: Recent advances and future challenges. PLoS Biol 22: e3002640, 2024.
40. Jemal A, Siegel R, Xu J and Ward E: Cancer statistics, 2010. CA Cancer J Clin 60: 277-300, 2010.
41. Broekman ML, Maas SL, Abels ER, Mempel TR, Krichevsky AM and Breakefield XO: Multidimensional communication in the microenvirons of glioblastoma. Nat Rev Neurol 14: 482-495, 2018.
42. Aldape K, Brindle KM, Chesler L, Chopra R, Gajjar A, Gilbert MR, Gottardo N, Gutmann DH, Hargrave D, Holland EC, *et al*: Challenges to curing primary brain tumours. Nat Rev Clin Oncol 16: 509-520, 2019.
43. The Cancer Genome Atlas Research Network: Comprehensive genomic characterization defines human glioblastoma genes and core pathways. Nature 455: 1061-1068, 2008.
44. Khabibov M, Garifullin A, Boumber Y, Khaddour K, Fernandez M, Khamitov F, Khalikova L, Kuznetsova N, Kit O and Kharin L: Signaling pathways and therapeutic approaches in glioblastoma multiforme (Review). Int J Oncol 60: 69, 2022.
45. Xie H, Li J, Lu M, Zhang R and Mao H: miR-1180 targets FXYD5 to regulate pancreatic cancer cells migration and invasion. Mol Biotechnol 66: 3182-3194, 2024.
46. Zhao E, Gao K, Xiong J, Liu Z, Chen Y and Yi L: The roles of FXYD family members in ovarian cancer: An integrated analysis by mining TCGA and GEO databases and functional validations. J Cancer Res Clin Oncol 149: 17269-17284, 2023.
47. Yao Y, Xue Y, Ma J, Shang C, Wang P, Liu L, Liu W, Li Z, Qu S, Li Z and Liu Y: MiR-330-mediated regulation of SH3GL2 expression enhances malignant behaviors of glioblastoma stem cells by activating ERK and PI3K/AKT signaling pathways. PLoS One 9: e95060, 2014.
48. Zheng X, Li W, Xu H, Liu J, Ren L, Yang Y, Li S, Wang J, Ji T and Du G: Sinomenine ester derivative inhibits glioblastoma by inducing mitochondria-dependent apoptosis and autophagy by PI3K/AKT/mTOR and AMPK/mTOR pathway. Acta Pharmaceutica Sinica B 11: 3465-3480, 2021.
49. Gasmi J and Sanderson JT: Growth inhibitory, antiandrogenic, and pro-apoptotic effects of punicic acid in LNCaP human prostate cancer cells. J Agric Food Chem 58: 12149-12156, 2010.
50. Wang L, Li W, Lin M, Garcia M, Mulholland D, Lilly M, Mulholland D, Lilly M and Martins-Green M: Luteolin, ellagic acid and punicic acid are natural products that inhibit prostate cancer metastasis. Carcinogenesis 35: 2321-2330, 2014.
51. Mete M, Unsal UU, Aydemir I, Sönmez PK and Tuglu MI: Punicic acid inhibits glioblastoma migration and proliferation via the PI3K/AKT1/mTOR signaling pathway. Anticancer Agents Med Chem 19: 1120-1131, 2019.
52. Lee J, Kotliarova S, Kotliarov Y, Li A, Su Q, Donin NM, Pastorino S, Purow BW, Christopher N, Zhang W, *et al*: Tumor stem cells derived from glioblastomas cultured in bFGF and EGF more closely mirror the phenotype and genotype of primary tumors than do serum-cultured cell lines. Cancer Cell 9: 391-403, 2006.
53. Lubarski I, Asher C and Garty H: Modulation of cell polarization by the Na+-K+-ATPase-associated protein FXYD5 (dysadherin). Am J Physiol Cell Physiol 306: C1080-C1088, 2014.
54. Fontana F, Giannitti G, Marchesi S and Limonta P: The PI3K/Akt pathway and glucose metabolism: A dangerous liaison in cancer. Int J Biol Sci 20: 3113-3125, 2024.